Hawaiian Picrite Basalt (ML647-2B) reactivity with CO_2-bearing solution on a micro-scale: Implications for carbon sequestration via mineral trapping

Cole B. Yeager

Advisor: Zhengrong Wang

Second Reader: Danny Rye

A senior thesis presented to the faculty of the Department of Geology & Geophysics, Yale University, in partial fulfillment of the Bachelor's Degree.

1. Abstract

Basalt has been targeted as a source rock for permanent geologic carbon sequestration and storage (CSS) due to its high dissolution rate of divalent cations, porosity, and permeability. However, few experiments have tested the carbonation fraction and extent of carbonate mineralization in whole-rock basalt samples exposed to CO_2-bearing solution under high-temperature/high-pressure conditions. The methods of this study include subjecting Hawaiian picrite basalt cubes (0.4cm x 0.4cm) to CO_2-bearing solution (0.5M and 1M $NaHCO_3$) at T=200 ºC and P=150 bar for 1, 5, and 10 days, and analyzing the reactions that took place in order to determine: 1) carbonation fraction (CF); 2) the extent of carbonate mineralization on the surface; 3) and the extent of carbonate mineralization within the rock. The extent of mineralization within the rock is important in determining the depth of carbonization reactions protruding past the solution-surface interface, which is a potential constraint surrounding practical carbon sequestration. Titration methods were conducted in order to assess the CF from these reactions; SEM and EDS analyses were carried out in order to visually identify any carbonate or secondary mineral precipitation on the surface of our reacted samples; and EPMA analysis was conducted on surfaces exposed by grinding ~0.1 cm into samples to understand the extent of mineralization beneath the surface. The results were matched against unreacted samples in order to identify any changes induced by the reactions. The CF measured was low ~0.2−2.0% for all samples, but my findings suggest that it increases with reaction time. SEM and EPMA analyses were unable to locate any carbonate minerals. Instead, secondary minerals (e.g. smectite, zeolite) formed extensively on the surface and to a lesser degree beneath the surface (on the basaltic matrix and rimmed around pore spaces). These findings suggest that solution strength, reaction time, and porosity are significant parameters affecting carbonate mineralization. Perhaps no carbonates were detected because of the re-dissolution of those initially formed, followed by the precipitation of secondary clay minerals. Permeability may constrain the ability of CO_2-bearing solution to permeate through the rock and find fresh surfaces to react with. Lastly, it is interesting to note that the location of the clay minerals beneath the original rock surface are constrained to basalt matrix vesicle and pore spaces, rather than on olivine phenocrysts. While earlier studies (Zhang, in preparation) have found that carbonate mineralization occurs mostly on olivine

surfaces, our results may provide insight that the re-dissolution of carbonates and precipitation of secondary clay minerals may not be as significant a constraint on practical carbon sequestration as originally believed given that they appear to prefer formation on different surfaces (olivine for carbonates, and basalt for secondary clays).

2. Introduction

2.1 Atmospheric CO_2:

Anthropogenic activities — such as fossil fuel combustion, iron and steel production, and cement manufacture — have led to a significant increase in atmospheric CO_2 concentration during our lifetime. CO_2 emissions are exponentially rising, and over the past 50 years alone atmospheric CO_2 has increased by 75 ppm, accounting for nearly 20% of total CO_2 content in the present atmosphere (390 ppm) (Mauna Loa Observatory: NOAA-ESRL). Currently, ~30 Gt/yr of CO_2 are being emitted from fossil fuel combustion, and this amount is projected to increase to ~43 Gt/yr by the year 2030 as developing nations advance in the transportation and electricity generation sectors (Broecker & Kunzig 2008; EIA 2009; Haszeldine 2009). Based on current growth scenarios, several studies project CO_2 concentrations on the order of 1100 ppm by the year 2100 (White et al. 2003; IPCC 2005, 2007). These high levels of anthropogenically-induced CO_2 are believed by many to cause global warming and climate change; thus, the reduction of CO_2 from the atmosphere has been a focal point in recent years and will be one of the main challenges of the future.

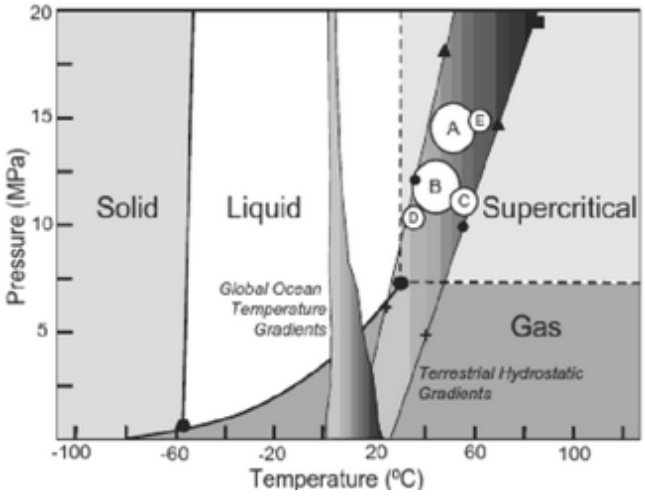

Figure 1: Phase behavior of CO_2 as a function of pressure and temperature, with stability fields representing ocean and hydrostatic pressure and temperature gradients (modified after Sundquist et al. 2009); (+) = 500m depth; (●) = 1000m depth; (▲) = 1500m depth; (■) = 2000m depth.

2.2 CO_2 Phase Relations and Solubility Behavior:

In the subsurface, CO_2 can exist as a dissolved component in groundwater, basinal brines, and geothermal fluids as well as in gaseous an liquid form. The physical state of CO_2 is dependent on temperature and pressure conditions as shown in Figure 1 (Hu et al. 2007;

Sundquist et al. 2009). At T = -55−31 ºC and P > 7.4 MPa (74 bar) CO_2 exists as a liquid, but at T > 31 ºC and P > 7.4 MPa (The T and P critical point) CO_2 is classified as a supercritical fluid. In the supercritical state, CO_2 behaves like a gas, but under high pressure the density of supercritical CO2 can be very high, approaching or even exceeding the density of liquid water (Kharaka & Cole 2011). For scenarios related to practical carbon sequestration, however, CO_2 is injected in liquid or gas form and transforms into supercritical fluid with depth as it is subjected to increased temperature and pressure in the reservoir.

After its injection into reservoirs, CO_2 can dissolve in water in accordance with:

$$CO_{2(g)} + H_2O = H_2CO_3$$

The product of this reaction, H_2CO_3, is aqueous carbonic acid, which can dissociate according to:

$$H_2CO_3 = HCO_3^- + H^+$$

A third reaction may take place in which bicarbonate, HCO_3^-, dissociates into carbonate and two hydrogen atoms:

$$HCO_3^- = CO_3^{2-} + 2H^+$$

This reaction liberates protons, causing the pH of the water to decrease. The pH of this solution will depend on the partial pressure of CO_2, temperature, alkalinity, and the salinity of water (Gislason et al. 2009). At pH values lower than ~6, carbonic acid (H_2CO_3) is the dominant carbonate species, with bicarbonate (HCO_3^-) and carbonate (CO_3^{2-}) becoming dominant at intermediate and high pH values, respectively. At conditions expected for most geologic sequestration sites (up to T=150 ºC and P=300 bar), the solubility of CO_2 increases, and thus the amount of water required for its dissolution decreases, with increasing CO_2 partial pressure, lower temperature, and lower salinity (Gislason et al. 2009).

A number of experimental and modeling studies have focused on the solubility of CO_2 in water at conditions relative to carbon storage (e.g. King et al. 1992; Spycher et al. 2003; Qin et al. 2008; Pappa et al. 2009). Upon initial injection, the CO_2-bearing fluid in the vicinity of the well is quite acidic, leading to increased reactivity with the host minerals. Those reactions typically cause an increase in pH that promotes a shift from $CO_{2(aq)}$-rich

fluid to fluid dominated by either HCO_3^- or CO_3^{2-}. Laboratory experiments by Czernichowski-Lauriol et al. 1996 have shown that CO_2 dissolution is rapid when the formation water and CO_2 share the same pore space, but once the formation fluid is saturated with CO_2, the uptake rate slows and is controlled by diffusion and convection rates. The principal benefit of CO_2 dissolution is that once it dissolves it no longer exists as a separate phase, thereby limiting the buoyant forces that may drive it upwards toward the surface following injection.

2.3 Carbon Sequestration Methods:

Geologic sequestration of CO_2 is considered a plausible option to reduce the greenhouse gas from the atmosphere. Sedimentary and igneous basins, depleted oil and gas wells, un-mineable coal seams, and deep saline aquifers have been investigated as possible reservoirs for bulk CO_2 injection (Hitchon 1996; Benson & Cole 2008; Goldberg et al. 2008; Kharaka et al. 2006, 2009; Gislason et al. 2009). Four possible CO_2-trapping mechanisms include: 1) structural trapping, whereby injected CO_2 is stored as a supercritical and buoyant fluid below a cap rock or impermeable stratum; 2) residual trapping of CO_2 by capillary forces in the pore spaces of reservoir rocks; 3) solution trapping, where CO_2 is dissolved in water and forms aqueous species such as H_2CO_3, HCO_3^-, and CO_3^{2-}; and 4) mineral trapping, with the CO_2 precipitating into carbonate minerals such as calcite ($CaCO_3$), dolomite ($CaMg(CO_3)_2$), magnesite ($MgCO_3$), siderite ($FeCO_3$), and dawsonite $NaAlCO_3(OH)_2$ (Gunter et al 1993; Palandri et al. 2005; Benezeth et al. 2007, 2009; Oelkers et al. 2008). One issue with the first three trapping mechanisms is that free gaseous or supercritical CO_2 may be subject to slow leakage (Dooley & Wise 2003), which will lower the effectiveness of sequestration. The fourth mechanism, 'mineral trapping', should serve as a more permanent CO_2 storage mechanism, which makes it a more promising approach. However, considerable uncertainties and scientific gaps exist in understanding the geochemistry surrounding CO_2-solution/mineral interactions at reservoir conditions (Kharaka et al. 2009; Haszeldine 2009), thus there is plenty of room for further experimentation and analysis.

2.3 Mineral Trapping by Carbonation

The potential effectiveness of storing atmospheric CO_2 in carbonate minerals is demonstrated by the relative volume of these minerals worldwide. While the total mass of carbon currently in the atmosphere is approximately 800 Gt, ~39,000,000 Gt of carbon are currently present in carbonate rocks, such as marble, limestone, and chalk in the Earth's crust (Oelkers & Cole 2008). For sequestering purposes, mineral carbonation involves the reaction of CO_2-solution with divalent cations (e.g. Mg^{2+}, Ca^{2+}, and Fe^{2+}) released from the reservoir rocks to form carbonates (e.g. calcite, dolomite, magnesite, Mg-Fe carbonates, and siderite). The process is comprised by a series of dissolution-precipitation reactions affected by CO_2-solution composition, reservoir rock composition, temperature, and pressure. Rocks rich in silicate minerals and glasses contain the most abundant cations available for dissolution and subsequent carbonate precipitation (Gislason et al. 2009).

Of all the silicate-containing rock formations, basalt is a promising choice for carbon sequestration for several reasons: 1) it contains a relatively abundant amount of divalent cations compared to other silicate-rich rocks; 2) the dissolution rate of basalt in reaction with CO_2-rich fluid is significantly greater than that of other silicate-rich rocks (e.g. granite); 3) basalt and other ultramafic rocks of similar quality are abundant and readily available on the terrestrial surface (e.g., Columbia River basalt and Deccan flood basalt) and are proven

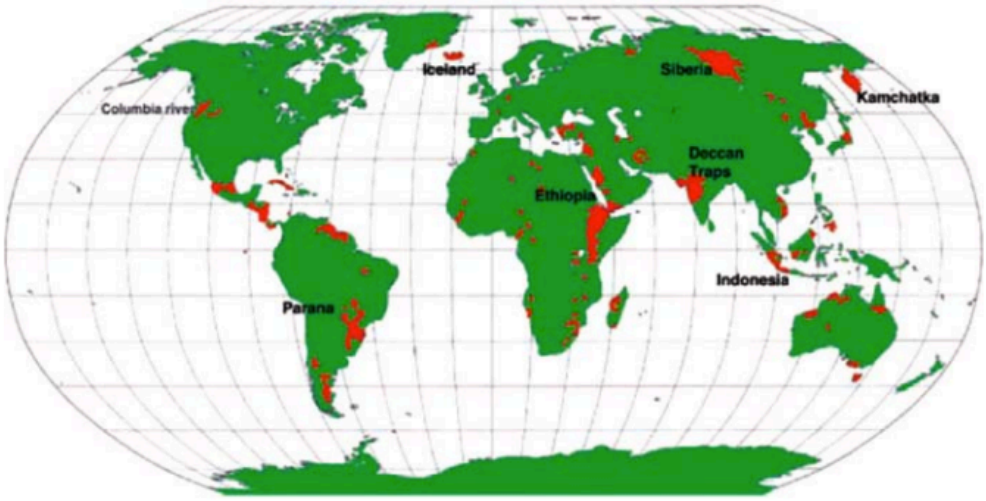

Figure 2:
Location of global terrestrial basalts (red) that could serve as in situ mineral carbonation sites (from Oelkers et al. 2008)

to be sufficient hosts for carbon sequestration (Figure 2); 4) basalt can attain high porosity and permeability, which allows CO_2 supercritical fluid to flow within the rock and increases the surface area available for reaction; and 5) low-permeability and impermeable massive basalt layers often cut through porous basalt bodies, thus providing a natural barrier for vertical CO_2 leakage (McGrail et al. 2006).

2.4 Active Carbon Sequestration Projects:

Currently there are a total of five commercial projects operating worldwide that capture and inject about seven million tons of CO_2 annually (Kharaka & Cole 2011). In addition, there are approximately 25 geologic sequestration field-demonstration projects in the U.S. at various stages of planning and development, and an equal number of projects are being implemented in other nations to investigate the storage potential of CO2 in various rock formations (saline aquifers, carbonates, basalts, and other ultra-mafics) using different injection schemes, monitoring methods, hazard assessment protocols, and mitigation strategies (Litynski et al. 2008; Cook 2009; Haszeldine 2009; Matter et al. 2009; Michael et al. 2009).

The CarbFix Pilot Project in Iceland is the world's first fully integrated CCS project with CO_2 storage in basaltic rocks. The project began in 2007 and was created to optimize CO_2 trapping via mineral carbonation. It involves the dynamic program of a CO_2 gas separation plant, CO_2 injection testing, laboratory-based experiments, and studies on numerical modeling. The CarbFix group has developed an injection system installed at the well for the purpose of CO_2 dissolution. The system runs at P=25 bar, and CO_2 and groundwater are injected together. The resulting fluid is carried to a depth of ~500 m where it enters the target storage formation fully dissolved (Matter et al. 2009). The amount of water required to fully dissolve the CO_2 depends on temperature and CO_2 partial pressure (expected pCO_2=25 bar). It is expected that the CO_2 charged water reacts with the basaltic minerals, resulting in a rising pH, increased alkalinity, and divalent cation dissolution/carbonate precipitation (Matter et al. 2009). The project is ongoing and aims to sequester up to 30,000 tons of CO_2 per year (Oelkers et al. 2008)

The Columbia River Flood basalt (CRFB) has been targeted as another potential source of CO_2 storage. It includes the Steen and Picture Gorge basalt formations in the

western U.S. and extends throughout Washington, Oregon, Idaho, and Nevada. The storage capacity at the CRFB has been estimated to be greater than 100 Gt CO_2 (McGrail et al. 2006), which is very significant given that current global fossil fuel and cement CO_2 emissions amount to ~30 Gt CO_2/yr (Friedlingstein et al. 2010).

3. Previous Work and Models on Carbonate Mineralization with Basalt

Mineral carbonation with basalt involves two processes: 1) basaltic mineral dissolution, which releases cations, and 2) carbonate precipitation, which captures carbon in minerals formed by reactions with the CO_2-fluid and divalent cations previously released from dissolution. A kinetic approach is necessary in dealing with mineral carbonation given that it encompasses irreversible heterogenous reactions. It involves dissolved CO_2 and silicate minerals as reactants, and carbonate minerals and Si-bearing minerals as products. Recent interest in CCS has led to an increasing number of laboratory experiments aimed at determining the many factors that affect the kinetics of dissolution and precipitation kinetics of several minerals. Unfortunately, few of these experiments have been performed under CO_2 partial pressures of interest for geological CO_2 sequestration. Furthermore, most of the obtained experimental rates are difficult to compare with one another due to their dependence on specific experimental apparatuses and varying conditions between researchers' experiments (eg. pH, temperature, solution composition and ionic strength, mineral composition, etc.) (Marini 2007, pp. 169). In spite of the incongruent nature of most experiments, the carbonate mineralization process can be interpreted theoretically by examining experimental results and applying them to broader geochemical modeling schemes.

3.1 Basalt Dissolution:

Typical basalt is mainly composed of calcic plagioclase feldspar, pyroxene, and olivine. Accessory minerals exist as various Fe- and Ti-oxides with minor interstitial glass. Our picrite basalt samples resemble a more typical tholeiitic composition, and our studies indicate that pyroxene may be represented by mostly augite, and plagioclase may be represented by mostly labradorite (see 4.1 'Samples' section). The different mineral

components of basalt display different dissolution characteristics during the irreversible heterogenous reactions with CO_2-bearing fluid.

Based on the results of many experimental studies conducted over the last ~25 years, silicate dissolution can be broken down into two steps: 1) a first step of non-stoichiometric dissolution due to the formation of a leached layer, followed by 2) a second step of steady-state, stoichiometric dissolution (Oelkers 2001).

According to Oelkers et al. (1994) and Oelkers (1996, 2001a), silicates and Al-silicates can be considered multi-oxides and their dissolution requires the breaking of more than one type of metal-oxygen bond. For this reason, the dissolution of silicates differs from that of simple oxides and hydroxides.

The dissolution process typically takes place through metal-proton exchange reactions by breaking the original metal-oxygen bonds and forming new proton-oxygen bonds. Of the silicates, nesosilicates have the simplest structure, made up of isolated SiO_4 tetrahedra, which makes their dissolution a rather simple process (Marini 2007). For example, forsterite dissolution takes place through the exchange of Mg^{2+} ions for protons. Breaking of the Mg-O bonds completely liberates the SiO_4 tetrahedra and there is no need to break any Si-O bonds for its dissolution. Casey (1991) has determined that the dissolution rates of nesosilicates are similar to those of simple oxides at constant temperature and pH.

The dissolution of other silicates, however, requires the breaking of more than one type of metal-oxygen bond. Dissolution for these minerals are thus more complicated because: 1) some of the metal-oxygen bonds break at different rates due to varying degrees of ionicity, and 2) some metals can be removed from the silicate structure before the mineral is totally dissolved (Marini 2007). Oelkers (2001) finds that these two occurrences cause a leached layer to form on these more complex silicates, specifically feldspars, wollastonite, and basaltic glass.

The rate of dissolution is limited by the slowest step in each reaction; in silicate dissolution this is the breaking of one kind of cation-oxygen bond. Several studies have

focused on the the dissolution mechanisms and rates of typical basalt minerals, including various feldspars, pyroxenes, oxides, and glass (Oelkers & Schott 1995; Oelkers 2001a; Oelkers & Schott 2001**;** Gislason & Oelkers 2003).

Kaolinite, enstatite, and wollastonite dissolution takes place in two separate phases: the first comprises a metal-proton exchange reaction involving Al^{3+} in kaolinite, Mg^{2+} in enstatite, and Ca^{2+} in wollastonite; the second is a reaction which breaks the Si-O bonds, thus completing dissolution (Marini 2007). The dissolution of alkali feldspars is more complicated as it involves three separate steps: 1) alkali ion-proton exchange, 2) Al^{3+} ion-proton exchange, and 3) breaking of the remaining Si-O bonds (Oelkers 2001). The dissolution of anorthite is simpler than that of alkali feldspars, as it requires one less step and consists of Ca^{2+} ion-proton exchange, followed by a second step of Al^{3+} ion-proton exchange. Similar to what is observed for forsterite, the breaking of the Ca-O and Al-O bonds causes complete destruction of the mineral lattice and Si-O bonds are not required to be broken in order to bring about dissolution (Marini 2007). Basaltic glass has the most complicated dissolution mechanism, in which protons sequentially exchange for alkalis, Ca^{2+}, Mg^{2+}, and Al^{3+} in that order; following these exchanges the remaining Si-O bonds can be broken (Oelkers 2001).

The following dissolution rates of typical basaltic end-member minerals are shown and described below. A is the pre-exponential factor, a_{H+} represents the proton activity, E_a is the apparent activation energy of the overall reaction, R is the universal gas constant, and T represents absolute temperature.

As olivine dissolves and silica is produced, protons are consumed, leading to an increase in pH. At conditions far from equilibrium, the dissolution for forsterite is independent of the Mg and Si concentrations in solution (Oelkers 2001). In an experimental study, the forsterite dissolution rate (r) was computed at temperatures ranging from 90−150 ℃ and pH ranging from 2−9.5 via the Arrhenius equation in Figure 3a:

$$r = Aa_{H+}^{n} \bullet \exp\left(\frac{-E_a}{RT}\right)$$

Figure 3a: Forsterite dissolution rate;
where A=0.0854 (+0.67 to -0.076), n=0.46 ± 0.03, and a_{H+}=52.9 ± 6.9 kJ/mol. (Hänchen et al. 2006)

Of the chain silicates, whose dissolution rates are poorly known, enstatite is the exception. Experiments on the dissolution rate for enstatite provide insight for those of other pyroxenes, which have similar structures involving the linkage of SiO_4 tetrahedra that share two of the four oxygen atom corners. These pyroxenes also provide insight for wollastonite, which is also a chain silicate. The steady-state dissolution rate of enstatite at far-from equilibrium conditions was determined by Oelkers & Schott (2001) at temperatures ranging from 28−168 ºC and pH ranging from 1−11 via the Arrhenius equation in Figure 3b:

$$r = A \bullet \exp\left(\frac{-E_a}{RT}\right) \bullet \left(\frac{a_{\mathrm{H}^+}^2}{a_{\mathrm{Mg}^{2+}}}\right)^n$$

Figure 3b: Enstatite dissolution rate;
where A=2.4 mol m^{-2} s^{-1}, E_a=48.5 kJ/mol, and n=0.125 (Oelkers & Schott 2001)

Feldspars are the most studied silicate minerals from the point of view of dissolution rates, and these investigations have greatly contributed to the general understanding of the dissolution kinetics of solid phases (Marini 2007). Due to the significant amount of labradorite in our ML647-2B picrite samples, its dissolution rate is portrayed below, however those of albite and K-rich feldspar have also been measured and may be more reliable. Carroll & Knauss (2005) measured the dissolution rate of labradorite ($An_{0.6}$) in solutions with temperature ranging from 30−130 ºC and pH close to 3.2. They found that the dissolution rate for labradorite was minimally affected by the presence of aqueous CO_2 and concluded that pH was the major controlling factor. Their results were combined into the Arrhenius equation in Figure 3c:

$$r = A \bullet \exp\left(\frac{-E_a}{2.303RT}\right) \bullet \left(\frac{(a_{\mathrm{H}^+}^2 / a_{Al^{3+}})^n \bullet K_T}{1 + K_T \bullet (a_{H^+}^3 / a_{Al^{3+}})^n}\right)$$

Figure 3c: Labradorite dissolution rate;
where A=$10^{-1.69}$ mol m^{-2} s^{-1}, and E_a=42.1 kJ/mol. Note that the thermodynamic equilibrium constant (K_T) is dependent on temperature. (Carrol & Knauss 2005)

As previously mentioned, dissolution of basaltic glass requires four sequential steps, and as a result the dissolution rates have been observed to be very slow (Oelkers 2001). The dissolution rate of basaltic glass was determined by Gislason & Oelkers (2003) by experiments under conditions with temperature ranging from 50−150 ºC and pH ranging from 2-11 (Figure 3d).

$$r = A \bullet \left(\frac{a_{H^+}^3}{a_{Al^{3+}}} \right)^n \bullet \exp\left(\frac{-E_a}{RT} \right)$$

Figure 3d: Basaltic Glass dissolution rate;
where A=$10^{-1.6}$ mol m^{-2} s^{-1}, E_a=25.5 kJ/mol, and n=0.66. (Gislason & Oelkers 2003)

The Arrhenius equations displayed in Figure 3 indicate that temperature and pH can significantly influence the dissolution rates of minerals in basalt. Higher temperatures lead to higher dissolution rates, however no linear relationship appears to exist between pH and dissolution rates. The dissolution rates for forsterite and enstatite will decrease monotonically with increasing pH levels. The dissolution rates for labradorite (and other plagioclases) and basaltic glass will also decrease with increasing pH levels at pH<7, however they will increase with increasing pH levels at pH>7 (Gudbrandsson et al. 2011).

The differences in dissolution rates between minerals that commonly exist in ultramafic rocks has been investigated by Gudbrandsson et al. (2011). Their data reveals that steady-state Ca (present in plagioclase) dissolution rates decrease with increasing pH under acidic conditions, but increase with increasing pH under alkaline conditions, while Mg and Fe (present in pyroxenes and olivine) dissolution rates decrease consistently with increasing pH levels. Their results show that plagioclase dissolution rates are slower than those of diopside at pH levels between 4−6, and slower than those of forsterite at pH<9 (Figure 4). For basaltic glass, they show

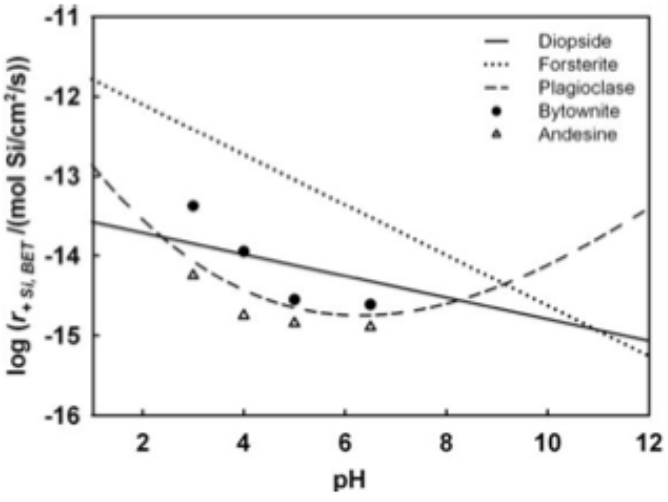

Figure 4: Si release rates of selected minerals at 25 ºC as a function of pH. (Gunbrandsson et al. 2011)

that Si dissolution rates are comparable to those of crystalline basalt with the same chemical composition at low pH levels and temperatures with T>25 ºC; however they are higher at high pH levels and temperatures with T>50 ºC. They conclude that the optimal dissolution rates for basaltic minerals occur under conditions of low pH and high temperature.

Other factors governing the dissolution rate of these minerals include CO_2-fluid composition, strength of bicarbonate solution, and simultaneous reactions of secondary mineral precipitation (Zhang, in preparation). Many studies have disagreed on whether or not secondary mineral precipitation either benefits or inhibits further the dissolution process of basaltic minerals. For example, Oelkers (2001) found that secondary mineral precipitation may allow protons to penetrate deeper into olivine faces, promoting continued dissolution. This belief is in agreement with Morrow et al. (2010), who confirm that secondary mineral precipitation on olivine surfaces causes the rapid release of Mg^{2+} ions. Other researchers, however, have suggested that the formation of secondary minerals on basalt mineral surfaces decreases their rate of dissolution (Grandstaff 1977; Béarat et al. 2006; Andreani et al. 2009; Garcia et al. 2010; King et al. 2010; Daval et al. 2011). These studies maintain it is possible that secondary mineral precipitation inhibits original mineral dissolution when a certain thickness covering the surface is reached (Jarvis et al. 2009). Stockmann et al. (2011) found that the presence of carbonate minerals on basaltic glass and diopside had no effect on the dissolution rates of the primary basaltic minerals, as the carbonates were rather porous, thus the cations still had a pathway to be removed. These results, and others (e.g. Cubillas et al. 2005) may indicate that crystallography plays a role in the early stages of the dissolution-precipitation process. In general, it is believed that strong CO_2-fluids and low secondary mineral precipitation lead to greater dissolution rates.

3.2 Carbonate Precipitation:

The kinetics of carbonate mineral precipitation has been significantly researched over the last several decades and remains an area of extreme interest due to its importance in many fields, such as in oil and gas operations, geothermal practices, fresh-water aquifer treatment, human buildings, and of course in geologic CO_2 storage. For CO_2 storage in basalt, interest lies with the dissolution of divalent cations from the basaltic minerals and their reaction with carbonic acid to form carbonates. During this process, the divalent cations will also be taken up by secondary minerals along with other cations (e.g. Al^{3+}, Na^{+}, and Si^{4+}). The precipitation of these secondary minerals will likely decrease the carbonation rate due to their competition with divalent cations to react with carbonic acid. In order to make carbonate mineralization as efficient as possible, it is necessary to limit the extent of secondary mineral precipitation. Carbonate mineralization is most likely to occur on olivine grains, given that olivine has the highest observed carbonation rate among basaltic minerals (Kelemen et al. 2011).

In nature, carbonate mineralization on basalt has been observed to occur via hydrothermal alteration (Gudmundsson & Arnórsson 2002 from Shuang) and basalt weathering (Gislason & Eugster 1987; Stefánsson & Gislason 2001). In the laboratory, carbonate dissolution-precipitation experiments are carried out by three methods: the pH-stat method, the rotating disk technique, and the channel-flow cell method. These experiments are dictated by the relatively fast reaction rates of carbonate minerals compared with silicates and oxides (for a detailed description of each of these methods, see Marini 2007 pp. 283). Many have utilized these methods to study coupled basalt dissolution-carbonate precipitation reactions (Nancollas & Reddy 1971; Sjöberg 1976; Reddy et al. 1981; Rickard & Sjöberg 1983; Gislason & Eugster 1987; Chou et al. 1989; Gislason et al. 1993, 2010; Pokrovsky & Schott 1999; McGrail et al. 2006; Matter et al. 2007; Oelkers 2008; Schaef et al. 2010; Gysi & Stefánsson 2012; Stockman et al. 2011; Rosenbauer et al. 2012). The following sections (3.2.1−3.2.7) are a compilation of some of their findings which demonstrate that several factors affect the precipitation of various carbonate minerals, such as: basalt composition, CO_2-fluid composition, temperature, pressure, oxygen fugacity, and reaction time.

3.2.1 Influence of Basalt Composition on Carbonate Precipitation:

The relatively high abundance of divalent cations in basalt theoretically contributes to its carbonate mineralization ability and high CF (Table 1). This observation has been confirmed by Rosenbauer et al. (2012), who found that the amount of CO_2-species uptake by basalt increases with its increasing abundance of Mg^{2+}. This observation suggests that the extent of carbonate mineralization is controlled by, and directly proportional to, bulk basalt magnesium content. Other studies, however, find that carbonate mineralization in basalt is variable and not proportional to divalent cation abundance. For instance, Schaef et al. (2010) conducted experiments under conditions of T=100 ºC, P=103 bar, and reaction times of up to one year; they found that the carbonation potential of different basalts varied and the bulk composition of basalt did not have a definitive influence on CF.

Rock Type	*Dunite*	*Basalt*	*Diorite*	*Andesite*	*Dacite*	*Granite*	*Rhyolite*
Mg^{2+}, Ca^{2+}, Fe^{2+} (wt. %)	32.98	**16.61**	10.91	10.12	6.03	3.04	1.95

Table 1:
Divalent cation (Mg^{2+}, Ca^{2+}, and Fe^{2+}) wt. % in common igneous rocks; (adapted from: Le Maitre 1976).

3.2.2 Influence of Temperature on Carbonate Precipitation in Basalt:

While basalt cation dissolution rates are significantly affected by temperature, the rate of carbonate precipitation with temperature has not been extensively studied. Gysi & Stefánsson (2012) conducted experiments in which basaltic glass was reacted with CO_2-bearing fluid at conditions of T=75 ºC, 150 ºC, and 250 ºC. Their findings suggest that carbonate mineralization is most favorable at 75 ºC, with Mg^{2+}, Ca^{2+}, and Fe^{2+} being incorporated into carbonates on the basalt surface. Additionally, they found that at higher temperatures of T=150 ºC and 250 ºC, secondary minerals (various clays and zeolites) were heavily prevalent and more eager to accept the basaltic divalent cations than carbonates.

This study, however, is not of uttermost importance given that interstitial basaltic glass is merely a trace component in most basalt, and the major components (such as plagioclase, pyroxene, and olivine) were not studied. More experiments must be done with these major basaltic components at constant pressure and variable temperature in order to better understand the effect temperature has on carbonate mineralization and secondary mineral precipitation/transformation.

3.2.3 Influence of Pressure on Carbonate Precipitation in Basalt:

While the partial pressure of CO_2 is a significant variable in CO_2 dissolution in water, few studies have tested its effect on carbonate precipitation in basalt. One significant consideration is that elevated CO_2 partial pressure increases the amount of aqueous CO_2 in the fluids that react with the dissolved basaltic divalent cations, which might theoretically increase the level of carbonate precipitation (Gysi & Stefánsson 2008). Roger et al. (2006) found that at elevated CO_2 conditions (from increased pressure), zeolites and clays were replaced by various carbonate minerals, such as siderite ($FeCO_3$), dolomite ($(CaMg)(CO_3)_2$), and magnesite ($MgCO_3$), as well as Si-minerals (eg. quartz (SiO_2)). These findings are promising for the increased ability of carbonates to precipitate on basalt at elevated pressures.

3.2.4 Influence of Oxygen Fugacity on Carbonate Precipitation in Basalt:

Gislason et al. (2010) find that reducing conditions increase CF with basalt given that reduced iron (Fe^{2+}) is more prevalent, and thus more available to react with CO_2 to form carbonate minerals. This means that carbonate mineralization on basalt is likely more efficient at low oxygen fugacity (fo_2), given that it leads to more reduced conditions. Oxygen fugacity as a parameter on carbonate precipitation has been minimally studied, and it may very well be a factor of limited importance.

3.2.5 Influence of pH on Carbonate Precipitation in Basalt:

The dissolution of basaltic divalent cations has been shown to be significantly affected by pH and the presence of protons (H^+) in solution, but its effect on carbonate

precipitation is also necessary to examine. Gysi & Stefánsson (2011) demonstrate that at relatively low pH levels (pH < 6.5) and low temperature, the mineralogy of precipitated minerals on the basalt surface after reaction consists of the secondary minerals quartz, Al-silicates, and Ca-Mg-Fe carbonates. Their studies also show that at higher pH levels (pH > 8), the mineralogy of precipitated minerals on the basalt surface after reaction consists of zeolites, calcite ($CaCO_3$), and Ca-Mg-Fe clays. These results indicate that competing reactions may exist between clays (Ca- and Fe- smectites), and carbonates at low pH levels, and between zeolites, clays (Mg- and Fe- smectites), and carbonates at high pH levels. Given the competition to precipitate between these minerals, it is likely that the available Ca^{2+}, Mg^{2+}, and Fe^{2+} ions are being "fought" for. Theoretically, if these ions can be made more widely available in the reacted solution, the effect of pH on carbonate and secondary mineral precipitation may be diminished and the conditions of pH for practical carbon sequestration may not be as significant a factor. However, given that elevated pH levels are necessary for optimal divalent cation dissolution, additional studies should be conducted that aim to increase the carbonate precipitation rate over that of secondary minerals under high pH conditions.

3.2.6 Influence of Reaction Time on Carbonate Precipitation in Basalt:

Reaction time appears to be a significant factor in terms of which minerals form on basalt. For instance, at the initial stage of cation dissolution and subsequent basalt alteration, hydrated SiO_2-minerals (e.g. opal, chalcedony, and quartz) tend to form on the surface environments (Stefánsson & Gislason 2001). The next set of minerals which tend to form shortly thereafter are Al-silicates (e.g. allophane, imogolite, kaolinite, or halloysite), followed by more complex minerals, such as smectite, zeolite, and carbonate (Stefánsson & Gislason 2001). The replacement of these more complex minerals by secondary minerals (e.g. clays and secondary zeolite) has also been observed, and should be further studied on time scales for practical carbon sequestration (e.g. multiple years) in order to better understand the exact timing with which the mineralogy may change.

3.2.7 Influence of CO_2-Fluid Composition on Carbonate Precipitation in Basalt:

The difficulty surrounding the composition of CO_2-fluid during carbon sequestration reactions exists in its differing effects on basalt cation dissolution and carbonate precipitation. Although acidic solutions (accompanied by low pH and high H^+ content) favor dissolution, carbonate precipitation probably responds better to alkaline solutions. Therefore, an optimal medium between the two must be met. Knauss et al. (2005) consider the additional presence of industrial waste components (e.g. SO_2 and H_2S) in solution for practical purposes. They find that the presence of H_2S has minimal effect on carbonate precipitation, however the presence of SO_2 can significantly alter carbonate precipitation, especially under oxidizing conditions due to the existence of very low pH fluids trapped in basaltic pore spaces. Furthermore, Schaef et al. (2010) find that the inclusion of H_2S in CO_2 supercritical fluid may enhance carbonate mineralization. Their studies focus on basalt native to the Karoo province and Columbia River Basin. However, their findings also indicate that the presence of H_2S negatively affected carbonation in the Newark Basin due to the precipitation of pyrite that appears to create a layer over the basalt surface, thus prohibiting contact between it and CO_2-fluid. Ideally, CO_2-fluid strength plays a large role in carbonate precipitation as well, and high CF values appear to correlate with high molarities of bicarbonate in solution.

4. Experimental Work

4.1 Samples:

The picrite basalts (ML647-2B) used in our experiments were collected in Hawaii. The hand specimen displays a porphyritic texture and contains many whole-grain olivine phenocrysts (with average diameters of ~1.5mm) set in a fine-grained basalt matrix of plagioclase and pyroxene. XRF analysis via the Siemens SRS-303 at the University of Hawaii indicates that the major picrite constituents are 45.8% SiO_2, 25.0% MgO, 13.3% Fe_2O_3, 7.5% Al_2O_3, 5.7% CaO, and 1.1% TiO_2. Trace constituents were Na_2O, K_2O, MnO, and P_2O_5 (Johnson, in preparation). The field-emission gun electron microprobe (JEOL JXA-8500F) was utilized in order to determine the average composition of the major minerals — olivine, plagioclase, and pyroxene. The average composition for olivine is $Mg_{1.72}Fe_{0.28}SiO_4$ (indicating mostly forsterite); for plagioclase is $Ca_{0.61}Na_{0.33}Al_{1.55}Si_{2.40}O_8$ (indicating

labradorite); and for pyroxene is $Mg_{1.11}Ca_{0.56}Fe_{0.34}Si_2O_6$ (indicating augite) (Zhang, in preparation).

Five thin sections were made of unreacted samples with thicknesses of ~400-500 μm so that the brittle olivine phenocrysts did not fracture or break off. These thin sections were scanned, the images were converted to 8-bit BMP files at 1000 pixels/inch, and they were run through a program called ImageJ with the macro file JPOR.txt to calculate total optical porosity (TOP) of the samples. The average TOP% of the five thin sections was calculated to be ~12.33%, however several researchers have found that this method is accompanied by a mean error variability of 3.5% (Grove & Jerram 2011), thus the TOP% of our samples were adjusted to range from ~11.9–12.8% (Table 2).

Thin Section	Total Pixels	Pixels Forming Porosity	Total Optical Porosity (TOP) %
TS1 (large)	2547853	295648	11.6391
TS2 (large)	2511036	327866	13.0570
TS3 (large)	2578104	344976	13.3810
TS4 (small)	251056	28449	11.3317
TS5 (small)	243750	29816	12.2322
Total Average	—	—	12.3282
Lower Average (with error variability)	—	—	~11.9
Upper Average (with error variability)	—	—	~12.8

Table 2:
Porosity calculations for five thin sections (3 large, and 2 small) using the ImageJ program with the macro file JPOR.txt; lower average and upper average calculations assume a mean error variability of ~3.5%.

Picrite cubes (0.4cm x 0.4cm) for SEM and EPMA analyses were cut using an ultra-thin diamond-encrusted saw blade. They were ground into cubic shape via a spinning wet wheel and 120 grit aluminum oxide abrasive compound. The cubes were then washed using ethanol and distilled water for several cycles before they were air dried for approximately one week and subsequently subjected to a CO_2-solution reaction under high

temperature and pressure in our autoclave at Yale University (process to be described in depth in section 4.2 'Methods').

4.2 Methods:

The picrite cubes, along with bicarbonate solution ($NaHCO_3$) of different volumes and different concentrations (0.5M and 1M), were weighed and added into gold capsules for reaction in our autoclave at Yale University (Figure 5). Bicarbonate solution volumes ranged from ~0.2–1 mL and cube weights ranged from ~0.7–0.15 g depending on the size and volumes of the available gold capsules. The gold capsules were sealed using the PUK 3S Professional plus Arc Welder and placed into the autoclave. The experiments were carried out under conditions of T=200 ºC and P=150 bar for durations of 1, 5, and 10 days. After each experiment, all gold capsules were quenched in distilled water at room temperature and then weighed again to check for any leakages. The solutions and solids in the capsules without any leakages were then collected; the solutions were centrifuged to remove any trace solids, and the larger solid products were washed in milli-Q water and ethanol for further analysis. The solid products were air dried for approximately one week and and analyzed via the scanning electron microscope (SEM) and energy-dispersive X-ray spectroscopy (EDS) at Yale University. An unreacted sample (named C-0) was also analyzed to determine baseline characteristics of the original rock from which comparisons of the reacted samples could be made.

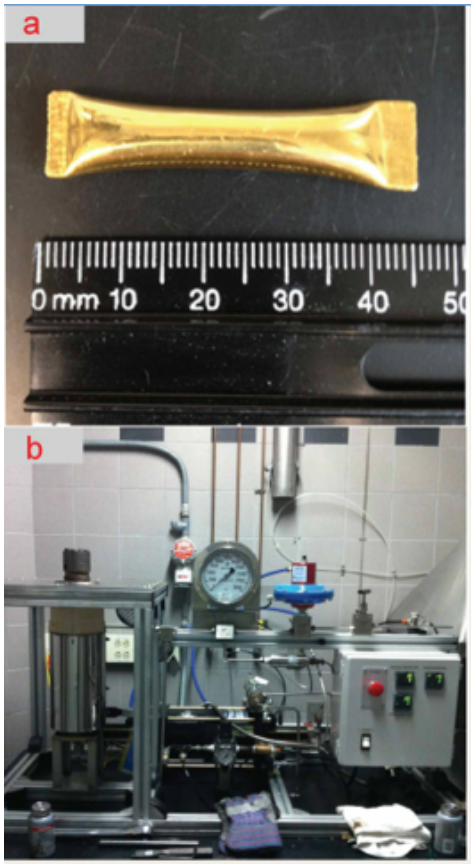

Figure 5:
a) Sealed gold capsule containing picrite cubes and bicarbonate solution
b) Auto clave at Yale University, West Campus

A titration method was used on the centrifuged solution to determine the CF of the picrite cubes after reaction with the CO_2-bearing fluid in the autoclave. Initial dissolved inorganic carbon (DIC) and final DIC were measured using the Mettler Toledo DL15 Titrator and the net change in DIC was taken to indicate the amount of carbonate mineral formation, from which we could calculate the CF of the picrite cubes. Before calculating the CF of the picrite cube samples, preliminary tests were carried out to ensure that the volume of the solution measured did not affect the accuracy of the titration results. These tests included the titration of 0.1 mL, 0.2 mL, 0.5 mL, and 0.8 mL standard $NaHCO_3$ solution, and the 1σ standard deviation was calculated to be ~0.5% for all volumes (Zhang, in preparation). We chose a solution volume of 0.1 mL to carry out the titration for the picrite samples given the small amount of CO_2-bearing solution (~0.2−1 mL) we used in our autoclave experiments.

One of the samples (C-5) was collected after SEM analysis, washed with ethanol, distilled water for several cycles, and later placed in cylindrical epoxy prisms which hardened after ~24 hours. It was then ground ~0.1cm into and subsequently polished using the Buehler Minimet 1000 Grinder-Polisher. It was polished against a micro-cloth sticker attached to a glass plate with a solution made of 0.05 μm aluminum oxide compound and mineral oil. It was then analyzed via the electron probe micro-analyzer (EPMA) at Yale University.

5. Experiment Results

5.1 CF of Samples via the Titration Method:

The CF of the picrite cube samples were calculated via the titration method and the following equations:

$$Mg^{2+} + Ca^{2+} + Fe^{2+} \text{ (consumed by wt.\%)} = \text{Initial DIC} - \text{Final DIC (in solution)}$$

$$CF = \frac{Mg + Ca + Fe \text{ (consumed by wt.\%)}}{Mg + Ca + Fe \text{ (in primary basalt)}}$$

The CF of samples with 0.5 M $NaHCO_3$ solution increased from 0.25% after 1 day to 0.52% after 5 days, and then held steady at 0.52% after 10 days. The CF of samples with 1 M $NaHCO_3$ solution increased from 0.06% after 1 day to 0.19% after 5 days, and then increased again to 2.30% after 10 days (which was the highest CF of all our reaction experiments). A graphical comparison of the CF between samples reacted with 0.5 M and 1 M $NaHCO_3$ is demonstrated in Figure 6.

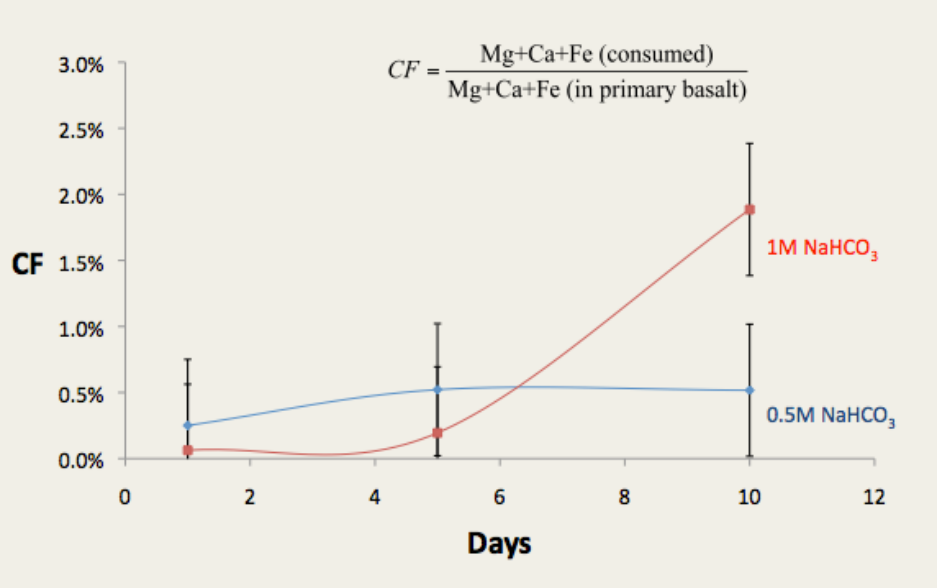

Figure 6:
A graph of the CF yielded by reaction between 0.5 M and 1 M $NaHCO_3$ solution with our picrite samples under conditions of T=200 ºC and P=150 bar over durations of 1, 5, and 10 days.

5.2 SEM & EDS Results:

SEM analysis was carried out for our picrite samples in order to examine where carbonates or secondary minerals precipitated on the surface. Our interests focused on the surfaces of olivine phenocrysts and the basalt matrix (plagioclase and pyroxene), as well as in pore spaces. While the CFs of our samples were determined to all be greater than 0%, no carbonates were found on any of our six samples. This observation is peculiar given that if any carbonates precipitated, they would likely be on the outermost surfaces rather than more deeply penetrated into the picrites. However, a significant amount of clay minerals (primarily smectite), and zeolite to a lesser extent, were detected by EDS on reacted samples. Both types of secondary minerals appeared to form mostly on the basalt matrix

rather than on olivine phenocrysts, whose surfaces were mostly clean. SEM images were also taken of the unreacted sample (C-0) so that a comparison could be made between the surfaces of unreacted and reacted picrites (Figure 7).

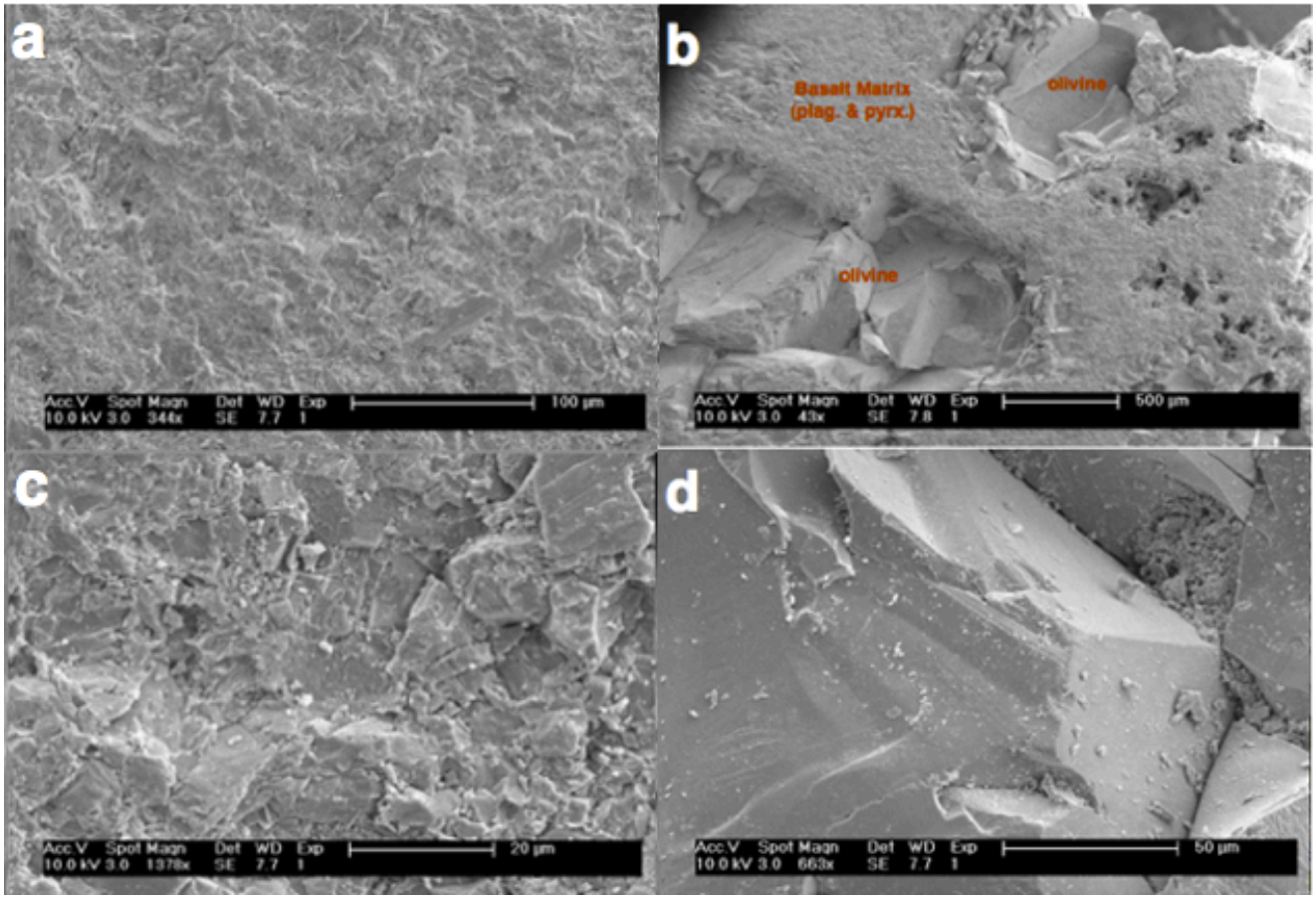

Figure 7: Unreacted Picrite Sample (C-0) SEM Images
a) The basalt matrix (plagioclase & pyroxene) at large scale (100 µm)
b) Olivine phenocrysts dispersed throughout the basalt matrix at large scale (500 µm)
c) The basalt matrix (plagioclase & pyroxene) at small scale (20 µm)
d) Olivine phenocryst at small scale (50 µm)

It is important to notice that the unreacted sample C-0 (Figure 7) displays no foreign mineralization on its surface. These images can be compared with the SEM images of reacted picrite samples (C-1, C-4, C-5, C-6, C-10, and C-11) in order to better understand the extent of mineralization on their surfaces (Figure 8). As previously noted, no carbonate mineralization was observed on any of these samples; instead we found a significant amount of secondary mineral precipitates, primarily in the form of clays and zeolite, but also Si-rich spherical minerals whose exact composition remains relatively unclear.

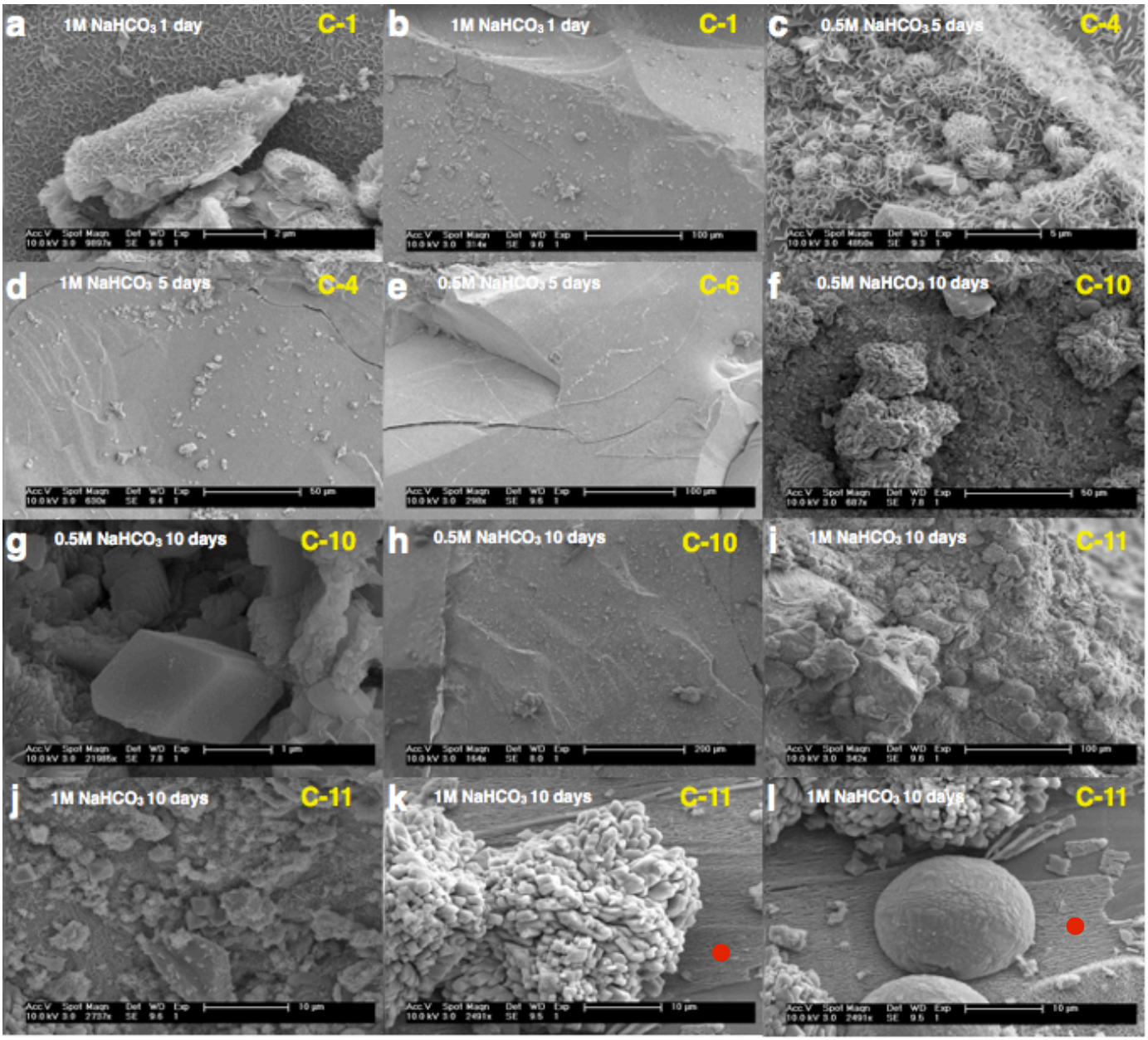

Figure 8:

a) C-1 sample (1 day rxn time) - Intermediate abundance of clay minerals (smectite) on basalt matrix surface at small scale (2 µm)
b) C-1 sample (1 day rxn time) - Clean olivine phenocryst surface with ~0 secondary mineral precipitation at large scale (100 µm)
c) C-4 sample (1 day rxn time) - Abundant clay mineral precipitates (smectite) on basalt matrix at small scale (5 µm)
d) C-4 sample (1 day rxn time) - Clean olivine phenocryst surface with ~0 secondary mineral precipitation at intermediate scale (50 µm)
e) C-6 sample (5 day rxn time) - Clean olivine phenocryst surface with ~0 secondary mineral precipitation at large scale (100 µm)
f) C-10 sample (10 day rxn time) - Dispersed secondary zeolite precipitation on basalt matrix at intermediate scale (50 µm)
g) C-10 sample (10 day rxn time) - Zeolite precipitate on basalt matrix at small scale (1 µm)
h) C-10 sample (10 day rxn time) - Clean olivine phenocryst surface with ~0 secondary mineral precipitation at large scale (200 µm)
i) C-11 sample (10 day rxn time) - Secondary mineral precipitation (smectite & Si-rich spheres) on basalt matrix at large scale (100 µm)
j) C-11 sample (10 day rxn time) - Abundant secondary mineral precipitates (smectite & zeolite) on basalt matrix at small scale (10 µm)
k) C-11 sample (10 day rxn time) - Unaltered plagioclase surrounded by clay mineral precipitate on basalt matrix at small scale (10 µm)
l) C-11 sample (10 day rxn time) - Si-rich sphere mineral surrounded by clay mineral precipitate on basalt matrix at small scale (10 µm)
*(Note: ● = unidentified clay mineral layer)

Figure 8b, 8d, 8e, and 8h demonstrate that foreign mineral precipitation (i.e. secondary clays, zeolite, and Si-rich minerals) did not extensively form on olivine surfaces throughout the 1, 5, and 10 day reactions. In fact, barely any of these minerals formed on the olivine surfaces at all. It is also important to notice that while a considerable amount of smectite formed on the basalt matrix after the 1 day reaction (Figure 8a; 8c), their abundance slightly decreased over the 5 and 10 day reactions. It appears that some of the smectite minerals may have undergone re-dissolution during the 5 and 10 day reactions, as zeolite becomes more prevalent on the basalt matrix (Figure 8f; 8g; 8j). The abundance of zeolite appears to increase with reaction time, as it exists minimally after the 1 day reaction, intermediately after the 5 day reaction, and more extensively after the 10 day reaction. This observation makes sense given that zeolite is a more complex mineral, and thus may require a longer time to precipitate.

A unidentifiable clay mineral also precipitated on the basalt matrix over the 10 day reaction (Figure 8k; 8l). While it appears to be visually different than smectite, EDS analysis indicates that it is also an Al-silicate clay mineral. Figure 8k shows its presence alongside plagioclase; and Figure 8l depicts it underneath a Si-rich sphere mineral, whose abundance increased with longer reaction times. EDS analysis calculated that the Si-rich sphere minerals possess a Si content >~60%, with minor amounts of Al. Figure 8i reveals several of these Si-rich spheres dispersed throughout the basalt matrix at a scale of 100 μm. The exact classification of these minerals is currently undetermined, however they seem to precipitate exclusively over layers of the unidentified clay minerals in samples C-10 and C-11.

5.3 EPMA Results:

EPMA analysis was carried out in order to determine: 1) an accurate quantitative composition of the picrites; 2) whether or not carbonation or secondary mineral precipitation occurred past the original rock surface-solution interface; 3) if there was any foreign mineralization, on which surfaces did it occur; 4) if any of the original minerals were altered by the dissolution of cations during reaction; and 5) if any cracks propagated throughout olivine grains as a result of the reaction.

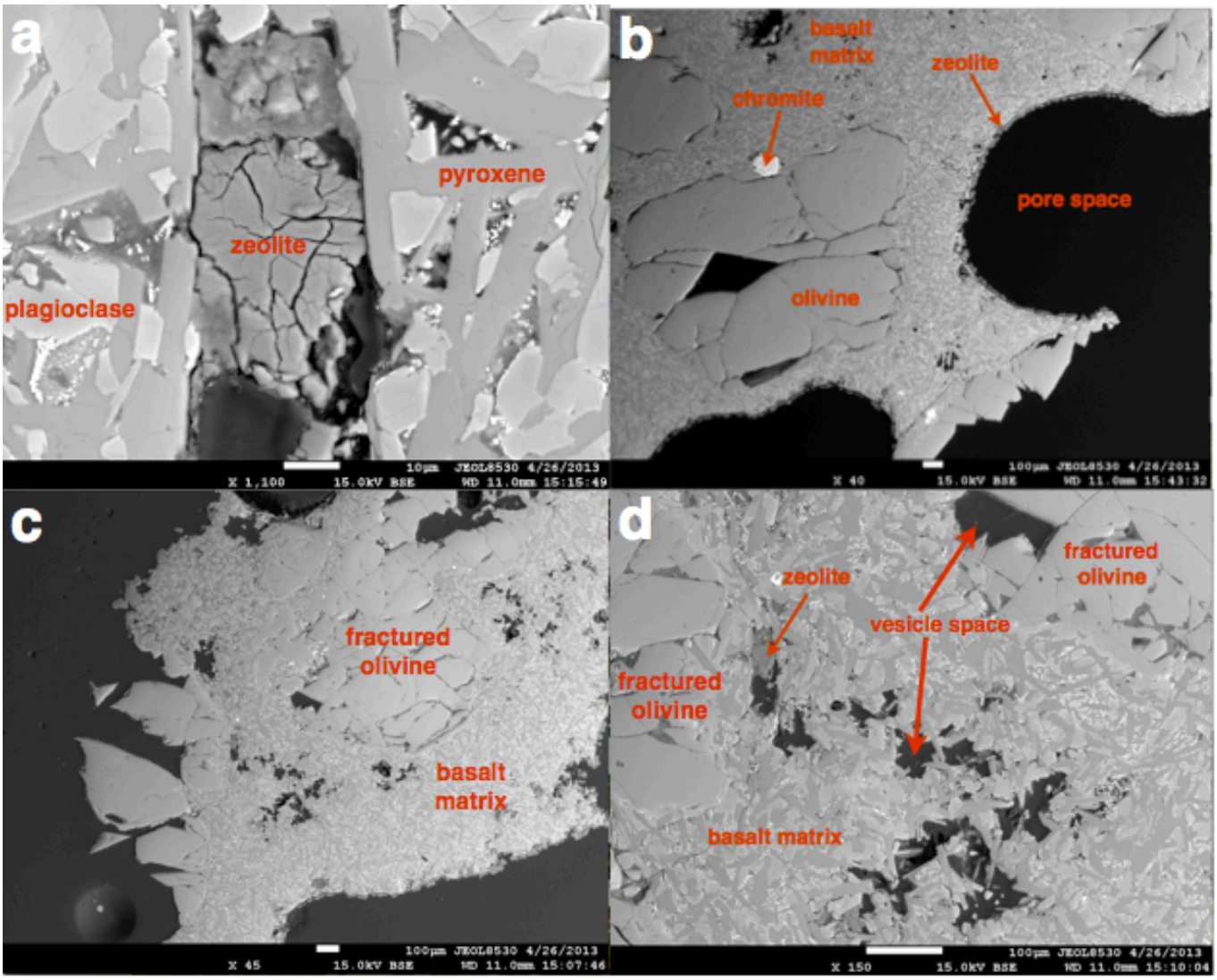

Figure 9: EPMA Image Analysis of C-5 Picrite Cube Sample (5 day rxn time; 1 M $NaHCO_3$ solution)
a) Na-zeolite (levyne-Na: $Na_2Al_2Si_4O_{12}•6H_2O$) in basalt matrix vesicle at small scale (10 μm); also seen at large scale in Figure 9d
b) Fractured olivine phenocryst, basalt matrix, chromite, and Na-zeolite (gmelinite-Na: $Na_4(Si_8Al_4)O_{24}•11H_2O$) rimmed around a pore space at large scale (100 μm)
c) Fractured olivine phenocryst amid the basalt matrix at large scale (100 μm)
d) Fractured olivine phenocryst, Na-zeolite seen in Figure 9a, basalt matrix, and vesicle spaces filled with epoxy at large scale (100 μm)

Similar to SEM analysis, EPMA analysis yielded no evidence of carbonate mineralization ~0.1 cm past the picrite surface. Again, this observation occurred despite the positive CF value (~0.19%) of sample C-5. We did notice, however, the presence of several Na-zeolites embedded in tiny basalt matrix vesicle spaces (~25μm x 100μm), as well as rimmed around pore spaces (Figure 9a and 9b, respectively). Two Na-zeolite types

were determined based on our collected elemental wt. % measurements; these were found to be levyne-Na (Figure 9a; formula: $Na_2Al_2Si_4O_{12}•6H_2O$) and gmelinite-Na (Figure 9b; formula: $Na_4(Si_8Al_4)O_{24}•11H_2O$). Our identification of these minerals may be further confirmed by the significant amount of water content we observed in them, and the fact that their chemical formulas show them to be typically quite hydrated.

The primary composition of the picrite was determined via EPMA to be a combination of feldspar, pyroxene, and olivine. Of the three data lines targeted on feldspar, the average composition was calculated to be mostly anorthite (65.6% with a standard deviation of 0.7%), albite (33.9% with a standard deviation of 0.6%), and minor orthoclase (0.6% with a standard deviation of 0.2%). Of the three data lines targeted on pyroxene, the average composition was calculated to be mostly enstatite (55.9% with a standard deviation of 0.6%), the pyroxenoid wollastonite (29.0% with a standard deviation of 1.1%), and ferrosilite (15.1% with a standard deviation of 0.7%). Of the thirteen data lines targeted on various olivine phenocrysts, the average composition was calculated to be mostly forsterite (83.7% with a standard deviation of 0.3%), as well as fayalite (16.3% with a standard deviation of 0.3%).

The main minerals (e.g. plagioclase, pyroxene, olivine) were found to not have been altered by the dissolution process during reaction. However, the olivine phenocrysts appeared to be extensively cracked. These cracks were filled with epoxy and did not propagate into the subophitic basalt matrix, indicating that they could have been a result of reaction and not as likely a result of grinding/polishing. However, one possibility is that they formed prior to collection from Hawaii and were perhaps initially cracked as a result of formation/tectonic stress or magmatic movement, and these cracks could have been further opened during our polishing process. We maintain that at least some partial cracking was a result of reaction in our autoclave.

6. Discussion:

6.1 Low CF for Picrite Cubes Compared to Similar Study for Picrite Powders

The low CF (Table 3) of our samples could have been a result of many factors. First, reaction duration may not be long enough, as in Figure 6 we see a significant incline in CF for 1 M $NaHCO_3$ solution from the 5 day to the 10 day reaction. Should experiments have been carried out on the duration of >10 days, perhaps we would have seen a CF increase in our picrite samples. Additionally, the strengths of the bicarbonate solution we used (0.5 M and 1 M) were likely too small. Another study on ML647-2B picrite powders reacted with 3 M NaHCO3 solution has shown to yield much higher CF values of up to 11.6% (Zhang, in preparation). This study demonstrates that surface area reactability is an important parameter for CF given that more of the CO2-bearing fluid may come into contact with the picrite samples. For instance, Zhang (in preparation) crushed ML647-2B picrite powders into grain sizes of 80−140 μm and 0−20 μm, reacted them with 3 M $NaHCO_3$ solution for 14 days in our Yale autoclave under the same conditions in my experiments (T=200 ºC, and P=150 bar) and witnessed CF values of 2.3% and 11.6%, respectively. A comparison between the highest CF values of our studies is depicted in Figure 10.

Sample #	NaHCO3 Solution Strength	Reaction Time	CF %
C-1	1 M	1 day	0.06%
C-4	0.5 M	1 day	0.25%
C-5	1 M	5 days	0.19%
C-6	0.5 M	5 days	0.52%
C-10	0.5 M	10 days	0.52%
C-11	1 M	10 days	2.30%

Table 3:
Our picrite cube samples (C-1, C-4, C-5, C-6, C-10, C-11); their reaction conditions and measured CF %

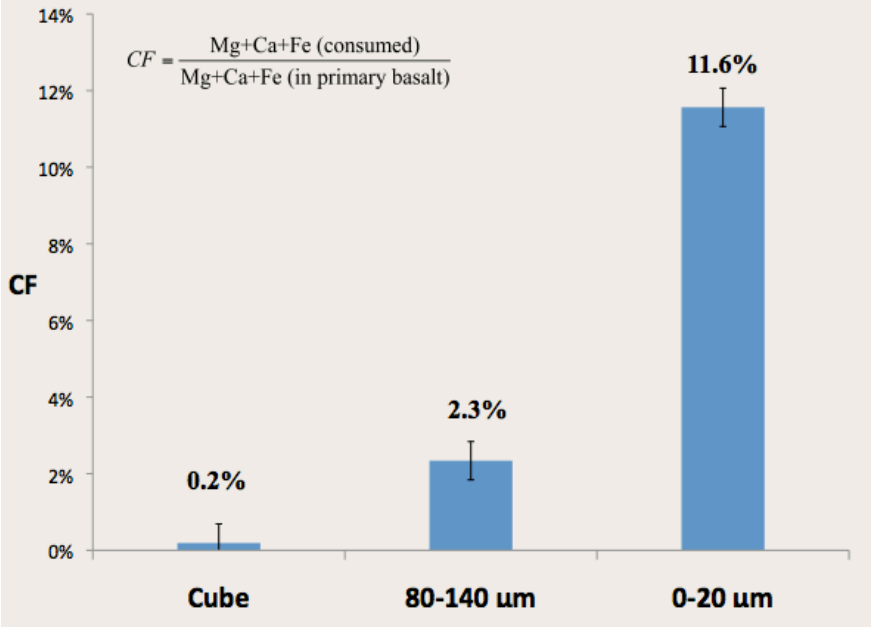

Figure 10:
A comparison of highest CF values from ML647-2B picrite cube (1 M NaHCO3; 10 day rxn time; this study) verse ML647-2B picrite powders of 80–140 µm and 0–20 µm (3 M NaHCO3; 14 day rxn time; Zhang, in preparation).

While our picrite cube samples yielded positive CF values from 0.06% to 2.30%, it is still possible that marginal to no carbonate precipitation actually occurred given the previously calculated 1σ standard deviation of ~0.5% (Zhang, in preparation). Given this standard deviation, our C-11 sample should have had some carbonate mineralization, however SEM analysis did not reveal any on the original surface, and EPMA analysis did not reveal any at ~0.1 cm depth past the original surface. While this observation is peculiar, our studies indicate that perhaps longer reaction times and stronger bicarbonate solution is required in order to achieve high CF values on picrite rocks due to limited surface area reactability and permeability.

6.2 Secondary Mineral Formation on Basalt Matrix and not Olivine Surfaces:

Our SEM analyses demonstrated that secondary minerals (smectite, zeolite, Si-rich minerals) formed extensively on the surface, however almost exclusively on the basalt matrix rather than on olivine phenocrysts, which were more or less completely clean. However, previous studies on our ML647-2B picrites (Zhang, in preparation) indicate that carbonate mineralization occurs primarily on the olivine phenocrysts. This occurrence provides insight that perhaps the typical secondary minerals (e.g. clays, zeolite, Si-rich minerals, etc.) may not compete with carbonates for precipitation on the same surfaces.

This observation is good for the practical purpose of CO_2 sequestration, given that many previous studies (see section 3.2 'Carbonate Precipitation') hypothesize that secondary minerals may compete with and replace previously formed carbonates on olivine surfaces.

Our EPMA analyses further confirm our observation that secondary minerals prefer formation on the basalt matrix. According to these analyses, at ~0.1 cm depth past the original surface-solution interface, zeolites formed exclusively within matrix vesicles and rimmed around pore spaces. These analyses also revealed that the olivine surfaces at ~0.1 cm depth were completely clean.

6.3 Cracked Olivine Grains from Reaction and the Implication for Higher CF Values:

Our EPMA images depict excessive cracks propagating throughout olivine phenocrysts at ~0.1 cm depth past the original surface-solution interface (Figures 9b; 9c; 9d). While the official cause of these cracks are relatively unknown, it appears that they were not a result of the grinding/polishing process given that they are completely filled with epoxy and do not extend into the subophitic matrix. While these cracks were not shown to be as extensive in our SEM images, perhaps they initiated at depth past the surface and were more easily revealed through the smoother 2D plane in our EPMA images as a result of polishing. It is also possible that these cracks have a much earlier physical origin, or were caused by previous stress/magmatic movement after their original formation.

We conclude that at least some of these cracks were partially caused by our reactions at high P/high T conditions in the autoclave, or as a result of dissolution/mineral precipitation. If this is the case, this observation is helpful for the practical purpose of CO_2 sequestration for two reasons: 1) the cracking of olivine phenocrysts during reaction will allow divalent cation (Mg^{2+}, Fe^{2+}) dissolution to extend deeper into the rock, thus making these cations more available in solution to react with carbonate species; and 2) as several studies have observed, carbonates prefer mineralization on olivine surfaces, thus the cracking of olivine phenocrysts during reaction will create more olivine surface area for carbonates to precipitate on.

6.4 Mineralization at Depths Shallower than ~0.1 cm Past Original Rock Surface:

EPMA analysis indicates that any mineral precipitation from the reactions appears to be minimal at depths of ~0.1 cm past the original picrite surface. While the sample we used for EPMA analysis was C-5, with a very low CF (0.19%), it is possible that no carbonates formed at all. However, secondary minerals (clays, zeolite, Si-rich minerals) were also not extensively revealed by EPMA. Additionally, the Na-zeolite rimmed around the pore spaces in Figure 9b was actually the corner of our sample and was part of the original surface with which the CO_2-bearing fluid came into direct contact. Few of these Na-zeolites were actually found at true ~0.1 cm depth past the original surface (one is depicted at small scale in Figure 9a, and at large scale in Figure 9d). This observation indicates that perhaps mineralization of secondary minerals and carbonates may occur at depths shallower than ~0.1 cm (e.g. ~0.01 cm, ~0.05 cm, etc.). The ~0.1 cm depth may be too deep for the dissolution/precipitation reactions to occur. This provides insight that for reaction times of 10 days and shorter and bicarbonate solution strengths of 1 M and smaller, dissolution and precipitation reactions may not extend much past the original surface. More experiments should be carried out at various shallower depths, longer reaction times, and with stronger bicarbonate solutions to determine exactly at which point these reactions halt past the original surface-solution interface.

7. Future Work and Conclusions

Future work on our ML647-2B picrite samples and other basalts will be carried out at Yale University for >3 years as part of the Carbon Sequestration Project. In the future we will update our autoclave to accommodate for fluid flow past our basalt samples to gain better insight on more practical reaction scenarios that take place under conditions of actual CO_2 sequestration in underground reservoirs. Additionally, the new autoclave will provide more space for our gold capsules, which are limited in size and incapable of containing high solution volumes and sample masses. Our ultimate goal is to determine how to decrease or inhibit the formation of secondary minerals to maximize the CF of our samples. Studies will be carried out that examine the effect of various conditions (pressure, temperature, solution composition, and solution strength) on mineral carbonation.

It is important to note that the 1 M $NaHCO_3$ solution we used in this study may be too low in strength. Previous studies have shown that 3 M $NaHCO_3$ solution tends to generate higher CF values and preferentially dissolves olivine, while 1 M $NaHCO_3$ solution tends to generate lower CF values and preferentially dissolves augite (Zhang, in preparation). Compared with olivine, augite and anorthite display low carbonation potentials, however these two minerals are the primary components of typical basalt. Therefore, experiments will be conducted that subject anorthite and augite to CO_2-bearing fluid under various conditions in order to better understand the carbonation mechanism of those two minerals.

Additionally EPMA analyses will be carried out that aim to determine the exact depth and extent of carbonate and secondary mineral precipitation beneath the original surface-solution interface, as well as the extent of mineral alteration by dissolution. Experiments will focus on several cross sections of our samples in order to examine any changes made by the reaction on multiple 2D planes. An additional focus will be the examination of the basalt matrix and olivine phenocrysts from rim to core to better understand the location of the reactions that take place.

Furthermore, while the porosity of our samples has been measured and is considered a parameter governing CO_2-fluid migration into basaltic rocks, permeability is likely a more significant factor. Thus, in the future it is essential to measure the permeability of our samples before and after reaction in the autoclave. These measurements will be able to determine exactly how important permeability is for carbonate mineralization, and will also reveal if post-reaction permeability is different than pre-reaction permeability.

Although no carbonate mineralization was observed in our analyses, this study deepens our understanding of secondary mineral precipitation mechanisms, the physical deformation of olivine as a result of reaction, the depth at which mineralization may occur past the original rock surface-solution interface, and the required strength of bicarbonate solution to induce carbonate mineralization. Our research can serve as a theoretical and

practical guide for sequestering CO_2 into ultramafic rocks. This study can be coupled with others of similar nature to better understand CO_2 sequestration via permanent carbonate mineral trapping to mitigate atmospheric CO_2, and thus reduce the risk of global climate change.

References

Andreani, M., Liquot, L., Gouze, P., Godard, M., Hoise, E., Gibert, B. 2009. Experimental study of carbon sequestration reactions controlled by the percolation of CO2-rich brine through peridioties. *Env. Sci. & Tech.*, vol. 43, pp. 1226-1241.

Bearat, H., McKelvey, M.J., Chizmeshya, A.V., Gormley, D., Nunez, R., Carpenter, R.W., Squires, K., Wolf, G.H. 2006. Carbon sequestration via aqueous olivine mineral carbonation: role of passivating layer formation. *Env. Sci. & Tech.*, vol. 40, pp. 4802-4808.

Benezeth, P., Palmer, A.D., Anovitz, L.M. and Horita, J. 2007. Dawsonite synthesis and re-evaluation of its thermodynamic properties from solubility measurements: Implications for mineral trapping of CO2. *Geochem. Cosmochim. Acta.*, vol. 71, pp. 4438-4455.

Benezith, P., Menez, B. and Noiriel, C. 2009. CO2 geological storage: Integrating geochemical, hydrodynamical, mechanical and biological processes from the pore to the reservoir scale. *Chem. Geol.*, vol. 265., pp. 1-2.

Benson, S.M. and Cole, D.R. 2008. CO2 sequestration in deep sedimentary formations. *Elements*, vol. 4 (5). In: DR Cole and EH Oelkers (eds.) Carbon Dioxide Sequestration. pp. 305-310.

Broecker, W.S. and Kunzig, R. 2008. CO2 Fixing Climate: What Past Climate Changes Reveal about the Current Threat –and How to Counter it. Hill and Wang, *New York*, pp. 253.

Carroll, S.A. and Knauss, K.G. 2005. Dependence of labradorite dissolution kinetics on CO2(aq), Al(aq), and temperature. *Chem. Geol.*, vol. 217, pp. 213-225.

Casey, W.H. 1991. On the relative dissolution rates of some oxide and orthosilicate minerals. *Journ. Colloid Interface Sci.*, vol. 146, pp. 586-589.

Chou, M., Garrels, R.M. and Wollast, R. 1989. Comparative study of the mechanics and mechanisms of dissolution of carbonate minerals. *Chem. Geol*., vol. 78, pp. 269-282.

Cook, P.J. 2009. Demonstration and Deployment of Carbon Dioxide Capture and Storage in Australia. *Energy Procedia*, vol. 1, pp. 3859-3866.

Cubillas, P., Kohler, S., Prieto, M., Causserand, C., Oelkers, E.H. 2005. How do domineral coatings affect dissolution rates? An experimental study of coupled CaCO3 dissolution –CdCO3 precipitation. *Geochem. Cosmochim. Acta*., vol. 69, pp. 5459-5476.

Czernichowski-Lauriol, I., Sanjuan, B., Rochelle, C., Bateman, K., Pearce, J. and Blackwell, P. 1996. The underground disposal of carbon dioxide. *Inorganic Geochemistry Journal*, vol. 27, pp. 183-276.

Daval, D., Sissman, O., Menguy, N., Saldi, G.D., Guyot, F., Martinez, I., Corviser, J., Garcia, B., Machouk, I., Knauss, K.G., Hellmann, R. 2011. Influence of amorphous silica layer formation on the dissolution rate of olivine at 90 ºC and elevated pCO2. *Chem. Geol.*, vol. 284, pp. 193-209.

Dooley, J.J. and Wise, M.A. 2003. Retention of CO2 in geologic sequestration formations: Desirable levels, economic considerations, and the implications for sequestration R&D. In: Proceedings of the Sixth International Conference on Greenhouse Gas Control Technologies, pp. 273-278.

Energy Information Administration (EIA). 2009. Annual Energy Outlook 2010 Early Release Overview. Report #:DOE/EIA-0383. Washington, D.C.

Friedlingstein, P., Houghton, R.A., Marland, G., Hackler, J., Boden, T.A., Conway, T.J., Canadell, J.G., Raupach, M.R., Ciais, P. and Le Quere, C. 2010. Update on CO2 emissions, *Nat. Geosci.*, vol. 3 (12), pp. 811-812.

Gislason, S.R., Wolff-Boenisch, D., Stefansson, A., Oelkers, E., Gunnlaugsson, E., Sigurdardottir, H., Sigfusson, Broecker, W., Matter, J., Stute, M., Axelsson, G. and Fridriksson, T. 2009. Mineral sequestration of carbon dioxide in basalt: The CarbFix project. *International Journal of Greenhouse Gas*, vol. 4, pp. 537-545.

Gislason, S.R., Eugster, H.P. 1987. Meteoric water-basalt interactions: A field study in N.E. Iceland. *Geochem. Cosmochim. Acta*., vol. 51, pp. 2841-2855.

Gislason, S.R., Veblen, D.R. and Livi, K.J.T. 1993. Experimental meteoric water-basalt interactions: characterization and interpretation of alteration products. *Geochem. Cosmochim. Acta*., vol. 57, pp. 1459-1471.

Gislason, S.R. and Oelkers, E.H. 2003. The mechanism, rates, and consequences of basaltic glass dissolution: An experimental study of the dissolution rates of basaltic glass as a function of pH at temperatures from 6 ºC to 150 ºC. *Geochem. Cosmochim. Acta*., vol. 67, pp. 3817-3832.

Goldberg, D.S., Takahashi, T. and Slagle, A.L. 2008. Carbon dioxide sequestration in deep-sea basalt. *Proc. Nat. Acad. Sci. U.S.A.*, vol. 105 (29), pp. 9925-9925.

Grandstaff, D.E. 1997. Some kinetics of bronzite orthopyroxene dissolution. *Geochem. Cosmochim. Acta*., vol. 41, pp. 1097-1103.

Gudbrandsson, S., Wolff-Boenisch, D., Gislason, S.R. and Oelkers, E.H. 2011. An experimental study of crystalline basalt dissolution from 2-6, 6-11 pH and temperatures from 5 to 75 ºC. *Geochem. Cosmochim. Acta*., vol. 75, pp. 5496-5509.

Gunter, W.D., Perkins, E.H. and McCann, T.J. 1993. Aquifer disposal of CO2-rich gases: reaction design for added capacity. *Energy Conversion and Management*, vol. 34, pp. 941-948.

Gysi, A.P. and Stefannson, A. 2008. Numerical modeling of CO2-water-basalt ineractions. *Miner. Mag*., vol. 72.

Gysi, A.P. and Stefannson, A. 2011. CO2-water-basalt interactions: Numerical simulations of low temperature CO2 sequestration into basalts. *Geochem. Cosmochim. Alta*., vol. 75, pp. 4728-4751.

Gysi, A.P. and Stefannson, A. 2012. Experiments and geochemical modeling of CO2 sequestration during hydrothermal basalt alteration. *Chem. Geol.*, vol. 306, pp. 10-28.

Haszeldine, S.R. 2009. Carbon Capture and Storage: How Green Can Black Be? *Science*, vol. 325, pp. 1647-1652.

Hitchon, B. 1996. *Aquifer Disposal of Carbon Dioxide*. Geoscience Publishing Ltd.., Sherwood Park, Alberta, Canada, pp. 165.

Hanchen, M., Prigiobbe, V., Storti, G., Seward, T.M. and Mazzotti M. 2006. Dissolution kinetics of forsteritic olivine at 90-150 ºC including effects of the presence of CO2. *Geochem. Cosmochim. Acta*., vol. 70, pp. 4403-4416.

Hu, J., Duan, Z., Zhu, C. and Chou, I.M. 2007. PVTx properties of the CO2-H2O and CO2-H2O-NaCl systems below 647 K: Assessment of experimental data and thermodynamic models. *Chem. Geol.*, vol. 238, pp. 249-267.

Keleman, P.B., Matter, J., Streit, E.E., Rudge, J.F., Curry, W.B., Blusztajn, J. 2011. Rates and mechanisms of mineral carbonation in peridotite: natural processes and recipes for enhanced, in situ CO2 capture and storage. *Ann. Rev. Earth Planet Sci*., vol. 39, pp. 545-576.

Kharaka, Y.K., Cole, D.R., Hovorka, S.D., Gunter, W.D., Knauss, K.G. and Freifield, B.M. 2006. Gas-water-rock interactions in Frio Formation following CO2 injection: implications to the storage of greenhouse gases in sedimentary basins. *Geology*, vol. 34. pp. 577-580.

Kharaka, Y.K., Thordsen, J.J. Hovorka, S.D., Nance, H.S., Cole, D.R., Phelps, T.J. and Knauss, K.G. 2009. Potential environmental issues of CO2 storage in deep saline aquifers: Geochemical results from the Frio-I Brine Pilot test, Texas, USA. *Applied Geochem.*, vol. 24 (6), pp. 1106-1112.

Kharaka, Y.K. and Cole, D.R. 2011. Geochemistry of Geologic Sequestration of Carbon Dioxide. In: *Frontiers in Geochemistry: Contribution of Geochemistry to the Study of the Earth,* First ed., pp. 149-174.

King, M.B., Murbarak, A., Kim, J.D. and Bott, T.R. 1992. The mutual solubilities of water with supercritical and liquid carbon dioxide. *Journ. Supercrit. Fluids*, vol. 5, pp. 296-302.

Knauss, K.G., Johnson, J.W. and Steffel, C.I. 2005. Evaluation of the impact of CO2, co-contaminant gas, aqueous fluid and reservoir rock interactions on the geologic sequestration of CO2. *Chem. Geol.*, vol. 217, pp. 339-350.

Litynski, J.T., Plasynski, S., McIlvried, H.G., Mahoney, C. and Srivastava, R.D. 2008. The United States Department of Energy's Carbon Sequestration Partnerships Program Validation Phase. *Environment International*, vol. 34, pp. 127-138.

Matter, J.M., Takahashi, T., Goldberg, D. 2007. Experimental evaluation of in situ CO2-water-rock reactions during CO2 injection in basaltic rocks: Implications for geological CO2 sequestration. *Geochem. Geophys. Geosyst.*, vol. 8.

Matter, J.M, Broecker, W.S., Stute, S., Gislason, S.R., Oelkers, E.H., Stefansson, A., Wolff-Boenisch, D., Gunnlaugsson, E., Axelson, G. and Bjornsson, G. 2009. Permanent Carbon Dioxide Storage into Basalt: The CarbFix Pilot Project, Iceland. *Energy Procedia*, vol. 1, pp. 3641-3646.

Marini, L. 2007. Geological Sequestration of Carbon Dioxide: Thermodynamics, Kinetics, and Reaction. Elsevier Publishing. Amsterdam, Netherlands, pp. 169-317.

McGrail, B.P., Schaef, H.T., Ho, A.M., Chien, Yi-Ju, Dooley, J.J., Davidson, C.L. 2006. Potential for carbon dioxide sequestration in flood basalts. *Journ. Geophys. Res.*, vol. 111.

Michael, K., Arnot, M., Cook, P., Ennis-King, J., Funnell, R., Kaldi, J., Kirsti, D. and Paterson, L. 2009. CO2 storage in saline aquifers: current state of scientific knowledge. *Energy Procedia*, vol. 1, pp. 3197-3204.

Nancollas, G.H. and Reddy M.M. 1971. The crystallization of calcium carbonate: Calcite growth mechanism. *Journ. Colloid Interface Sci*., vol. 37, pp. 824-830.

Oelkers, E.H. and Schott, J. 1995. Experimental study of anorthite dissolution and the relative mechanism of feldspar hydrolysis. *Geochem. Cosmochim. Acta*., vol. 59, pp. 5039-5053.

Oelkers, E.H. 1996. Physical and chemical properties of rocks and fluids for chemical mass transport calculations. In: Lichtner, P.C., Steefel, C.I. and Oelkers, E.H. (eds.) *Reactive Transport in Porous Media*, *Reviews in Mineralogy*, Mineralogical Society of America, vol. 34, pp. 131-191.

Oelkers, E.H., Schott, J. and Devidal, J.L. 1994. The effect of aluminim, pH, and chemical affinity on the rates of aluminosilicate dissolution reactions. *Geochem. Cosmochim. Alta*., vol. 58, pp. 2011-2024.

Oelkers, E.H., 2001. General kinetic description of multioxide silicate mineral and glass dissolution. *Geochem. Cosmochim. Acta.*, vol. 65, pp. 3703-3719.

Oelkers, E.H. and Schott, J. 2001. An experimental study of enstatite dissolution rates as a function of pH, temperature, and aqueous Mg and Si concentration, and the mechanism of pyroxene/pyroxenoid dissolution. *Geochem. Cosmochim. Alta*., vol. 65, pp. 1219-1231.

Oelkers, E.H. and Cole, D.R. 2008. Carbon dioxide sequestration: A solution to a global problem. *Elements*, vol. 4, pp. 305-310.

Oelkers, E.H., Gislason, S.R. and Matter, J. 2008. Mineral Carbonation of CO2. *Elements*, vol. 4 (5), pp. 333-337.

Pappa, G.D., Perakis, C., Tsimpanogiannis, I.N. and Voutsas, E.C. 2009. Thermodynamic modeling of the vapor-liquid equilibrium of the CO2/H2O mixture. *Fluid Phase Equil*., vol. 284, pp. 56-63.

Palandri, J.L., Rosenbauer, R.J. and Kharaka, Y.K. 2005. Ferric iron in sediments as a novel CO2 mineral trap: CO2-SO2 reaction with hematite. *Applied Geochem.*, vol. 20, pp. 2038-2048.

Pokrovsky, O.S. and Schott, J. 1999. Processes at the magnesium-bearing carbonates/ solution interface: Kinetics and mechanism of magnesite dissolution. *Geochem. Cosmochim. Acta*., vol. 63, pp. 881-897.

Qin, J., Rosenbauer, R.J. and Duan, Z. 2008. Experimental Measurements of Vapor-Liquid Equilibria of the H2O + CO2 + CH4 Ternary System. *Journ. Chem. Eng. Data.*, vol. 53, pp. 1246-1249.

Reddy, M.M., Plummer, L.N. and Busenberg, E. 1981. Crystal growth of calcite from calcium bicarbonate solution at constant PCO2 and 25 ºC. A test of calcite dissolution model. *Geochem. Cosmochim. Alta*., vol. 45, pp. 1281-1289.

Rickard, D.T. and Sjoberg, E.L. 1983. Mixed kinetic control of calcite dissolution rates. *Am Journ. Sci*., vo. 283, pp. 815-830.

Roger, K.L., Neuhoff, P.S., Pedersen, A.K. and Bird, D.K. 2006. CO2 metasomatism in a basalt-hosted petroleum reservoir, Nuussuaq, West Greenland. *Lithos*., vol. 92, pp. 55-82.

Rosenbauer, R.J., Thomas, B., Bischoff, J.L. and Palandri, J. 2012. Carbon sequestration via reaction with basaltic rocks: geochemical modeling and experimental results. *Geochem. Cosmochim. Alta*., vol. 89, pp. 116-133.

Schaef, H.T., McGrail, B.P., and Owen, A.T. 2010. Carbonate mineralization of volcanic province basalts. *Int. Journ. Greenhouse Gas Control*., vol. 4, pp. 249-261.

Sjoberg, E.L. 1976. A fundamental equation for calcite dissolution kinetics. *Geochem. Cosmochim. Acta*., vol. 40, pp. 441-447.

Spycher, N., Pruess, K. and Ennis-King, J. 2003. CO2-H2O mixtures in geologic sequestration of CO2: Assessment and calculation of mutual solubilities from 12 to 100 ºC and up to 600 bar. *Geochem. Cosmochim. Acta.*, vol. 67, pp. 3015-3031.

Stefansson, A., Gislason, S.R. 2001. Chemical weathering of basalts, SW Iceland: effect of rock crystallinity and secondary minerals on chemical fluxes to the ocean. *Am. Journ. Sci*., vol. 301, pp. 513-556.

Stockmann, G.J., Wolff-Boenisch, D., Gislason, S.R. and Oelkers, E.H. 2011. Do carbonate precipitates affect dissolution kinetics? 1: basaltic glass. *Chem. Geol.*, vol. 284, pp. 306-316.

Sundquist, E.T., Ackerman, K.V., Parker, L. and Huntzinger, D.N. 2009. An Introduction to the Global carbon Cycle. In: BJ McPherson and ET Sundquist (eds.) *Carbon Sequestration and Its Role in the Global Carbon Cycle*. American Geophysical Union, Geophysical Monograph 183, Washington, D.C., pp. 1-23.

White, C.M, Strazisar, B.R. and Granite, E.J. 2003. Separation and capture of CO2 from large stationary sources and sequestration in geologic formations: coalbeds and deep saline aquifers. *Journal of Air & Waste Management Association*, vol. 53, pp. 647-715.

Zhang, S. (in preparation). Thermodynamics and Kinetics of Mineral Carbonation. Yale University Major Thesis Proposal.